Regulation of Store-Operated Ca^{2+} Entry by IP_3 Receptors Independent of Their Ability to Release Ca^{2+}

Pragnya Chakraborty[1,2], Bipan Kumar Deb[1,3], Colin W. Taylor[4,*] and Gaiti Hasan[1,5,*]

[1]National Centre for Biological Sciences, Tata Institute of Fundamental Research, Bellary Road, Bangalore, 560065, India.

[2]SASTRA University, Thanjavur, Tamil Nadu, 613401, India.

[3]Present address: Department of Molecular and Cell Biology, University of California, Berkeley, CA, 94720, USA.

[4]Department of Pharmacology, University of Cambridge, Cambridge, CB2 1PD, UK.

[5]Lead Contact

[*]Correspondence: cwt1000@cam.ac.uk, gaiti@ncbs.res.in

ABSTRACT

Loss of ER Ca^{2+} activates store-operated Ca^{2+} entry (SOCE) by causing STIM1 to unfurl domains that activate Orai1 channels in the plasma membrane at membrane contact sites (MCS). In human neurons, SOCE evoked by thapsigargin to deplete ER Ca^{2+} is attenuated by loss of IP_3Rs, and restored by expression of IP_3Rs even when they cannot release Ca^{2+}, but only if the IP_3Rs can bind IP_3. In cells expressing pore-dead IP_3Rs, IP_3 enhances SOCE evoked by partial store depletion without enhancing Ca^{2+} release. Proximity ligation assays establish that IP_3Rs enhance association of STIM1 with Orai1 in cells with empty stores; this requires an IP_3-binding site, but not a pore. Over-expressing STIM1, or extended synaptotagmin-1 to exaggerate MCS, circumvents the need for IP_3Rs. Thus, IP_3 binding to IP_3Rs stimulates SOCE by both mediating ER Ca^{2+} release and promoting STIM1-Orai1 interactions. Convergent regulation by IP_3Rs may tune SOCE to respond selectively to IP_3.

Keywords: Ca^{2+} signaling, extended synaptotagmin, human neural progenitor cell, IP_3 receptor, membrane contact site, neuron, Orai, proximity ligation assay, STIM, store-operated Ca^{2+} entry

INTRODUCTION

The activities of all eukaryotic cells are regulated by increases in cytosolic free Ca^{2+} concentration ($[Ca^{2+}]_c$), which are almost invariably evoked by the opening of Ca^{2+}-permeable ion channels in biological membranes. The presence of these Ca^{2+} channels within the plasma membrane (PM) and the membranes of intracellular Ca^{2+} stores, most notably the endoplasmic reticulum (ER), allows cells to use both intracellular and extracellular sources of Ca^{2+} to evoke Ca^{2+} signals. In animal cells, the most widely expressed Ca^{2+} signaling sequence links extracellular stimuli, through their specific receptors and activation of phospholipase C, to formation of inositol 1,4,5-trisphosphate (IP_3), which then stimulates Ca^{2+} release from the ER through IP_3 receptors (IP_3R) (Foskett *et al.*, 2007; Prole and Taylor, 2019). IP_3Rs occupy a central role in Ca^{2+} signaling by releasing Ca^{2+} from the ER. IP_3Rs thereby elicit cytosolic Ca^{2+} signals, and by depleting the ER of Ca^{2+} they initiate a sequence that leads to activation of store-operated Ca^{2+} entry (SOCE) across the PM (Putney, 1986; Thillaiappan *et al.*, 2019). SOCE occurs when loss of Ca^{2+} from the ER causes Ca^{2+} to dissociate from the luminal Ca^{2+}-binding sites of an integral ER protein, stromal interaction molecule 1 (STIM1). STIM1 then unfolds its cytosolic domains to expose a region that binds directly to a Ca^{2+} channel within the PM, Orai, causing it to open and Ca^{2+} to flow into the cell across the PM (Parekh and Putney, 2005; Prakriya and Lewis, 2015; Lewis, 2020). The interactions between STIM1 and Orai occur across a narrow gap between the ER and PM, a membrane contact site (MCS), where STIM1 puncta trap Orai channels. While STIM1 and Orai are undoubtedly the core components of SOCE, many additional proteins modulate their interactions (Rosado,

Jenner and Sage, 2000; Palty *et al.*, 2012; Deb, Pathak and Hasan, 2016; Srivats *et al.*, 2016) and other proteins contribute by regulating the assembly of MCS (Chang *et al.*, 2013; Giordano *et al.*, 2013; Kang *et al.*, 2019).

It is accepted that IP_3-evoked Ca^{2+} release from the ER through IP_3Rs is the usual means by which extracellular stimuli evoke SOCE. Here, the role of the IP_3R is widely assumed to be restricted to its ability to mediate Ca^{2+} release from the ER and thereby activate STIM1. Evidence from *Drosophila*, where we suggested an additional role for IP_3Rs in regulating SOCE (Agrawal et al., 2010; Chakraborty et al., 2016), motivated the present study, wherein we examined the contribution of IP_3Rs to SOCE in mammalian neurons. We show that in addition to their ability to activate STIM1 by evoking ER Ca^{2+} release, IP_3Rs also facilitate interactions between active STIM1 and Orai1. This additional role for IP_3Rs, which is regulated by IP_3 but does not require a functional pore, reveals an unexpected link between IP_3, IP_3Rs and Ca^{2+} signaling that is not mediated by IP_3-evoked Ca^{2+} release. We speculate that dual regulation of SOCE by IP_3Rs may allow Ca^{2+} release evoked by IP_3 to be preferentially coupled to SOCE.

RESULTS

Loss of IP_3R1 Attenuates SOCE in Human Neural Stem Cells and Neurons

We investigated the effects of IP_3Rs on SOCE by measuring $[Ca^{2+}]_c$ in human neural stem cells and neurons prepared from embryonic stem cells. Human neural progenitor cells (hNPCs) were derived from H9 embryonic stem cells using small molecules that mimic cues provided during human brain development (Gopurappilly *et al.*, 2018). We

confirmed that hNPCs express canonical markers of neural stem cells (**Figure 1A**) and that IP_3R1 is the predominant IP_3R subtype (GEO accession no. GSE109111) (Gopurappilly *et al.*, 2018). An inducible lentiviral shRNA-miR construct targeting IP_3R1 reduced IP_3R1 expression by 93 ± 0.4% relative to a non-silencing (NS) construct (**Figures 1B and 1C**). Carbachol stimulates muscarinic acetylcholine receptors, which are expressed at low levels in hNPCs (Gopurappilly *et al.*, 2018). In Ca^{2+}-free medium, carbachol evoked an increase in $[Ca^{2+}]_c$ in about 10% of hNPCs, consistent with it stimulating Ca^{2+} release from the ER through IP_3Rs. Restoration of extracellular Ca^{2+} then evoked an increase in $[Ca^{2+}]_c$ in all cells that responded to carbachol. Both carbachol-evoked Ca^{2+} release and SOCE were abolished in hNPCs expressing IP_3R1-shRNA, confirming the effectiveness of the IP_3R1 knockdown (**Figures S1A-S1C**).

Thapsigargin, a selective and irreversible inhibitor of the ER Ca^{2+} pump (sarcoplasmic/endoplasmic reticulum Ca^{2+}-ATPase, SERCA), was used to deplete the ER of Ca^{2+} and thereby activate SOCE (**Figure 1D**) (Parekh and Putney, 2005). Restoration of extracellular Ca^{2+} to thapsigargin-treated hNPCs evoked a large increase in $[Ca^{2+}]_c$, reflecting the activity of SOCE (**Figure 1D**). The maximal amplitude and rate of SOCE were significantly reduced in cells lacking IP_3R1, but the resting $[Ca^{2+}]_c$ and thapsigargin-evoked Ca^{2+} release were unaffected (**Figures 1D-1F** and **Figures S1D and S1E**). STIM1 and Orai1 expression was also unaltered in hNPC lacking IP_3R1 (**Figure S1G**). After spontaneous differentiation of hNPC, cells expressed markers typical of mature neurons, and the cells responded to depolarization with an increase in $[Ca^{2+}]_c$ (**Figures S1F and S1H-S1J**). Thapsigargin

evoked SOCE in these differentiated neurons; and expression of IP_3R1-shRNA significantly reduced the SOCE response without affecting depolarization-evoked Ca^{2+} signals (**Figures 1H-1J** and **Figures S1H-S1L**).

Loss of IP_3R1 Attenuates SOCE in Human Neuroblastoma Cells

IP_3Rs link physiological stimuli that evoke Ca^{2+} release from the ER to SOCE, but the contribution of IP_3Rs is thought to be limited to their ability to deplete the ER of Ca^{2+}. We have reported that in *Drosophila* neurons there is an additional requirement for IP_3Rs independent of ER Ca^{2+} release (Venkiteswaran and Hasan, 2009; Agrawal *et al.*, 2010; Chakraborty *et al.*, 2016). Our results with hNPCs and stem cell-derived neurons suggest a similar requirement for IP_3Rs in regulating SOCE in mammalian neurons. To explore the mechanisms underlying this additional role for IP_3Rs, we turned to a more tractable cell line, SH-SY5Y cells. These cells are derived from a human neuroblastoma; they exhibit many neuronal characteristics (Agholme *et al.*, 2010); they express M3 muscarinic acetylcholine receptors that evoke IP_3-mediated Ca^{2+} release and SOCE (Grudt, Usowicz and Henderson, 1996); and they express predominantly IP_3R1 (Wojcikiewicz, 1995; Tovey *et al.*, 2001), with detectable IP_3R3, but no IP_3R2 (**Figure 2A**). We used inducible expression of IP_3R1-shRNA to significantly reduce IP_3R1 expression (by 74 ± 1.2%), without affecting IP_3R3 (**Figures 2A and 2B**). As expected, carbachol-evoked Ca^{2+} signals in individual SH-SY5Y cells were heterogenous and the carbachol-evoked Ca^{2+} release was significantly reduced by knockdown of IP_3R1 (**Figures 2C and 2D** and **Figures S2A and S2B**). Thapsigargin evoked SOCE in SH-SY5Y cells (Grudt, Usowicz and Henderson, 1996),

and it was significantly attenuated after knockdown of IP_3R1 without affecting resting $[Ca^{2+}]_c$, the Ca^{2+} release evoked by thapsigargin or expression of STIM1 and Orai1 (**Figures 2E-2G** and **Figures S2C-S2E**). We also used CRISPR/Cas9n to disrupt one copy of the IP_3R1 gene in SH-SY5Y cells with an associated decrease in IP_3R1 expression and attenuation of carbachol-evoked Ca^{2+} signals (**Figures S2F-S2I**). In these cells, thapsigargin-evoked Ca^{2+} release was minimally perturbed, but the resulting SOCE was much reduced (**Figures S2J and S2K**). These observations, which replicate those from hNPCs and neurons (**Figure 1**), vindicate our use of SH-SY5Y cells to explore the mechanisms linking IP_3Rs to SOCE in human neurons.

Expression of IP_3R1 or IP_3R3 in SH-SY5Y cells expressing IP_3R1-shRNA restored both carbachol-evoked Ca^{2+} release and thapsigargin-evoked SOCE without affecting resting $[Ca^{2+}]_c$ or thapsigargin-evoked Ca^{2+} release (**Figures 2H-2J** and **Figures S3A-S3D**). Over-expression of STIM1 in cells expressing NS-shRNA had no effect on SOCE (**Figures S3E and S3F**), but it restored thapsigargin-evoked SOCE in cells expressing IP_3R1-shRNA, without affecting resting $[Ca^{2+}]_c$ or thapsigargin-evoked Ca^{2+} release (**Figures 2K-2M**). We conclude that IP_3Rs are required for optimal SOCE, but they are not essential because additional STIM1 can replace the need for IP_3Rs (**Figure 3A**).

It has been reported that SOCE is unaffected by loss of IP_3R in non-neuronal cells (Ma *et al.*, 2001; Chakraborty *et al.*, 2016). Consistent with these observations, the SOCE evoked in HEK 293T cells by stores emptied fully by treatment with thapsigargin was unaffected by expression of IP_3R1 shRNA (**Figures S4A-S4C**) or by knockout of all three IP_3R subtypes using CRISPR/cas9 (**Figures S4D and S4E**).

Neuronal and non-neuronal cells may, therefore, differ in the contribution of IP_3R to SOCE. We return to this point later.

Binding of IP_3 to IP_3R Without a Functional Pore Stimulates SOCE

IP_3Rs are large tetrameric channels that open when they bind IP_3 and Ca^{2+}, but they also associate with many other proteins (Prole and Taylor, 2019), and many IP_3Rs within cells appear not to release Ca^{2+} (Thillaiappan *et al.*, 2019). A point mutation (D2550A, $IP_3R1^{D/A}$) within the IP_3R1 pore prevents it from conducting Ca^{2+} (Dellis *et al.*, 2008). As expected, expression of $IP_3R1^{D/A}$ in cells lacking IP_3R1 failed to rescue carbachol-evoked Ca^{2+} release, but it unexpectedly restored thapsigargin-evoked SOCE (**Figures 3B-3D** and **Figures S5A-S5E**). We confirmed that rescue of thapsigargin-evoked Ca^{2+} entry by this pore-dead IP_3R was mediated by a conventional SOCE pathway by demonstrating that it was substantially attenuated by siRNA-mediated knockdown of Orai1 (**Figures 3C and 3D** and **Figures S5F-S5H**).

Activation of IP_3Rs is initiated by IP_3 binding to the N-terminal IP_3-binding core of each IP_3R subunit (Prole and Taylor, 2019). Mutation of two conserved phosphate-coordinating residues in the α-domain of the binding core (R568Q and K569Q of IP_3R1, $IP_3R1^{RQ/KQ}$) almost abolishes IP_3 binding (Yoshikawa *et al.*, 1996; Iwai *et al.*, 2007), while mutation of a single residue (R568Q, IP_3R1^{RQ}) reduces the IP_3 affinity by ~10-fold (Dellis *et al.*, 2008). Expression of rat $IP_3R1^{RQ/KQ}$ rescued neither carbachol-evoked Ca^{2+} release nor thapsigargin-evoked SOCE in cells lacking IP_3R1 (**Figures 3E and 3F** and **Figure S5C)**. However, expression of IP_3R1^{RQ} substantially rescued thapsigargin-evoked SOCE (**Figures 3E and 3F** and **Figures S5I and S5J**).

Expression of an N-terminal fragment of rat IP_3R (IP_3R1^{1-604}), to which IP_3 binds normally (Iwai *et al.*, 2007), failed to rescue thapsigargin-evoked SOCE (**Figures S5K and S5L)**. These results establish that a functional IP_3-binding site within a full-length IP_3R is required for IP_3Rs to facilitate thapsigargin-evoked SOCE. Hence in cells with empty Ca^{2+} stores, IP_3 binding, but not pore-opening, is required for regulation of SOCE by IP_3Rs. In cells stimulated only with thapsigargin and expressing IP_3Rs with deficient IP_3 binding, basal levels of IP_3 are probably insufficient to meet this need.

We further examined the need for IP_3 by partially depleting the ER of Ca^{2+} using cyclopiazonic acid (CPA), a reversible inhibitor of SERCA, to allow submaximal activation of SOCE (**Figures S5M and S5N**). Under these conditions, addition of carbachol in Ca^{2+}-free HBSS to cells expressing IP_3R1-shRNA caused a small increase in $[Ca^{2+}]_c$ (**Figures 4A-4C**). In the same cells expressing IP_3R1^{DA}, the carbachol-evoked Ca^{2+} release was indistinguishable from that observed in cells without IP_3R^{DA} (**Figures 4B and 4C**), indicating that the small response was entirely mediated by residual native IP_3R1 and/or IP_3R3. Hence, the experiment allows carbachol to stimulate IP_3 production in cells expressing IP_3R1^{DA} without causing additional Ca^{2+} release. The key result is that in cells expressing IP_3R1^{DA}, carbachol substantially increased SOCE (**Figures 4A-4C**). We conclude that IP_3, through IP_3Rs, regulates coupling of empty stores to SOCE. This is the first example of an IP_3R mediating a response to IP_3 that does not require the pore of the channel.

G-protein-coupled receptors are linked to IP_3 formation through the G-protein Gq, which stimulates phospholipase C β (PLC β). We used YM-254890 to inhibit Gq

(Kostenis, Pfeil and Annala, 2020; Patt *et al.*, 2021). As expected, addition of YM-254890 to wild type (WT) or NS-shRNA transfected SH-SY5Y cells abolished the Ca^{2+} signals evoked by carbachol, but it also reduced the maximal amplitude and rate of thapsigargin-evoked SOCE (**Figures 4D- 4E** and **Figure S5O**). YM-254890 had no effect on the residual thapsigarign-evoked SOCE in SH-SY5Y cells expressing IP_3R1-shRNA **(Figure 4F** and **Figure S4O**). The latter result is important because it demonstrates that the inhibition of SOCE in cells with functional IP_3Rs is not an off-target effect causing a direct inhibition of SOCE.

In HEK 293T cells, YM-254890 had no effect on thapsigargin-evoked SOCE, but it did inhibit SOCE in HEK 293T cells lacking IP_3R1 (**Figures 4G-4I** and **Figures S6C-S6E**). These results suggest that in HEK 293T cells, which express all three IP_3R subtypes (Mataragka & Taylor, 2018), neither loss of IP_3R1 nor inhibition of Gαq is sufficient on its own to inhibit thapsigargin-evoked SOCE, but when combined there is a synergistic loss of SOCE.

IP_3Rs Promote Interaction of STIM1 With Orai1 Within MCS

Our evidence that IP_3Rs intercept coupling between empty stores and SOCE (**Figure 3A**) prompted us to investigate the coupling of STIM1 with Orai1 across the narrow junctions between ER and PM (Carrasco and Meyer, 2011). An *in situ* proximity ligation assay (PLA) is well suited to analyzing this interaction because it provides a signal when two immunolabelled proteins are within ~40 nm of each other (Derangère *et al.*, 2016), a distance comparable to the dimensions of the junctions wherein STIM1 and Orai1 interact (Poteser *et al.*, 2016). We confirmed the specificity of the PLA and

demonstrated that it reports increased association of STIM1 with Orai1 after treating SH-SY5Y cells with thapsigargin (**Figure 5A** and **Figures S7A-S7F**). In cells expressing IP_3R1-shRNA, thapsigargin had no effect on the STIM1-Orai1 interaction reported by PLA, but the interaction was rescued by expression of IP_3R1 or IP_3R1^{DA}. There was no rescue with $IP_3R1^{RQ/KQ}$ (**Figures 5B-5E**). The results with PLA exactly mirror those from functional analyses (**Figures 1** and **2**), suggesting that IP_3 binding to IP_3R enhances SOCE by facilitating interaction of STIM1 with Orai1 (**Figure 3A**).

Extended synaptotagmins (E-Syts) are ER proteins that stabilize ER-PM junctions including STIM1-Orai1 MCS (Maléth *et al.*, 2014; Kang *et al.*, 2019; Woo *et al.*, 2020). Over-expression of E-Syt1 in SH-SY5Y cells expressing IP_3R1-shRNA rescued thapsigargin-evoked Ca^{2+} entry without affecting resting $[Ca^{2+}]_c$ or thapsigargin-evoked Ca^{2+} release (**Figures 6A-6C**). The rescued Ca^{2+} entry is likely to be mediated by conventional SOCE because it was substantially attenuated by knockdown of STIM1 (**Figures 6D-6F)**. Over-expression of E-Syt1 had no effect on SOCE in cells with unperturbed IP_3Rs (**Figures 6G-6I**). These results suggest that attenuated SOCE after loss of IP_3Rs can be restored by exaggerating ER-PM MCS.

DISCUSSION

After identification of STIM1 and Orai1 as core components of SOCE (Prakriya and Lewis, 2015; Thillaiappan *et al.*, 2019), the sole role of IP_3Rs within the SOCE pathway was assumed to be the release of ER Ca^{2+} that triggers STIM1 activation. The assumption is consistent with evidence that thapsigargin-evoked SOCE can occur in avian (Sugawara *et al.*, 1997; Ma *et al.*, 2002; Chakraborty *et al.*, 2016) and

mammalian cells without IP_3Rs (Prakriya and Lewis, 2001). Although SOCE in mammalian HEK 293T was unaffected by loss of IP_3Rs in our study (**Figure 4G and 4I)**, it was modestly reduced in other studies of mammalian cells (Bartok *et al.*, 2019; Yue *et al.*, 2020). However, additional complexity is suggested by evidence that SOCE may be reduced in cells without IP_3Rs (Chakraborty *et al.*, 2016; Bartok *et al.*, 2019; Yue *et al.*, 2020), by observations implicating phospholipase C in SOCE regulation (Rosado, Jenner and Sage, 2000; Broad *et al.*, 2001), by evidence that SOCE responds differently to IP_3Rs activated by different synthetic ligands (Parekh, Riley and Potter, 2002) and by some, albeit conflicting reports (Ahmad *et al.*, 2022), that IP_3Rs may interact with STIM and/or Orai (Woodard *et al.*, 2010; Santoso, Cebotaru and Guggino, 2011; Béliveau, Lessard and Guillemette, 2014; Sampieri *et al.*, 2018).

We identified two roles for IP_3Rs in controlling endogenous SOCE in human neurons. As widely reported, IP_3Rs activate STIM1 by releasing Ca^{2+} from the ER, but they also, and independent of their ability to release Ca^{2+}, enhance interactions between active STIM1 and Orai1 (**Figure 7**). The second role for IP_3Rs can be supplanted by over-expressing other components of the SOCE complex, notably STIM1 or ESyt1 (**Figures 2K-2M** and **Figures 6A and 6B**). It is intriguing that STIM1 (Carrasco and Meyer, 2011; Lewis, 2020), ESyt1 (Giordano *et al.*, 2013) and perhaps IP_3Rs (through the IP_3-binding core) interact with phosphatidylinositol 4,5-bisphosphate (PIP_2), which is dynamically associated with SOCE-MCS (Kang *et al.*, 2019). We suggest that the extent to which IP_3Rs tune SOCE in different cells is probably determined by the strength of Gq signaling and endogenous interactions

between STIM1 and Orai1. The latter is likely to depend on the relative expression of STIM1 and Orai1 (Woo *et al.*, 2020), the STIM isoforms expressed, expression of proteins that stabilize STIM1-Orai1 interactions (Darbellay *et al.*, 2011; Rana *et al.*, 2015; Rosado *et al.*, 2016; Knapp *et al.*, 2020), and the size and number of the MCS where STIM1 and Orai1 interact (Kang *et al.*, 2019). The multifarious contributors to SOCE suggest that cells may differ in whether they express "spare capacity". In neuronal cells, loss of IP_3 (**Figure 4D**) or of the dominant IP_3R isoform (IP_3R1-shRNA; **Figures 1 and 2**) is sufficient to unveil the contribution of IP_3R to SOCE, whereas HEK 293Tcells require loss of both IP_3 and IP_3R1 to unveil the contribution (**Figures 4H and 4I**). The persistence of SOCE in cells devoid of IP_3Rs (**Figures S4D and S4E**) (Prakriya and Lewis, 2001; Ma *et al.*, 2002) probably arises from adaptive changes within the SOCE pathway. This does not detract from our conclusion that under physiological conditions, where receptors through IP_3 initiate SOCE, IP_3Rs actively regulate SOCE.

The IP_3Rs that initiate Ca^{2+} signals reside in ER immediately beneath the PM and alongside, but not within, the MCS where STIM1 accumulates after store depletion (Thillaiappan *et al.*, 2017). In migrating cells too, IP_3Rs and STIM1 remain separated as they redistribute to the leading edge (Okeke *et al.*, 2016). Furthermore, there is evidence that neither STIM1 nor STIM2 co-immmunoprecipitate with IP_3R1 (Ahmad *et al.*, 2022). We suggest, and consistent with evidence that SOCE in cells without IP_3Rs can be restored by over-expressing E-Syt1 (**Figures 6A-6C**), that IP_3Rs probably facilitate SOCE by stabilizing the MCS wherein STIM1 and Orai1 interact, rather than by directly regulating either protein. This proposal provides an analogy with similar

structural roles for IP_3Rs in maintaining MCS between ER and mitochondria (Bartok *et al.*, 2019) or lysosomes (Atakpa *et al.*, 2018) (**Figure 7**). Since both contributions of IP_3Rs to SOCE require IP_3 binding (**Figures 3E and 3F**), each is ultimately controlled by receptors that stimulate IP_3 formation (**Figures 4B and 4C**). Convergent regulation by IP_3Rs at two steps in the SOCE pathway may ensure that receptor-regulated PLC activity provides the most effective stimulus for SOCE; more effective, for example, than ryanodine receptors, which are also expressed in neurons. By opening IP_3Rs parked alongside SOCE MCS (Thillaiappan *et al.*, 2017; Ahmad *et al.*, 2022), IP_3 selectively releases Ca^{2+} from ER that is optimally placed to stimulate SOCE, and by facilitating Orai1-STIM1 interactions IP_3 reinforces this local activation of SOCE (**Figure 7**).

We conclude that IP_3-regulated IP_3Rs regulate SOCE by mediating Ca^{2+} release from the ER, thereby activating STIM1 and/or STIM2 (Ahmad *et al.*, 2022) and, independent of their ability to release Ca^{2+}, IP_3Rs facilitate the interactions between STIM and Orai that activate SOCE. Dual regulation of SOCE by IP_3 and IP_3Rs allows robust control by cell-surface receptors and may reinforce local stimulation of Ca^{2+} entry.

ACKNOWLEDGEMENTS

This research was supported by grants to G.H. from the Dept. of Biotechnology, Govt. of India (BT/PR6371/COE/34/19/2013) and NCBS-TIFR core support, and to C.W.T. from the Wellcome Trust (101844) and Biotechnology and Biological Sciences Research Council (BB/T012986/1). P.C is supported by a DST-INSPIRE fellowship

(DST/INSPIRE Fellowship/2017/IF170360) and she received an Infosys-NCBS travel award to visit C.W.T.'s lab at Cambridge. We are grateful to Renjitha Gopurappilly (NCBS, TIFR) for the derivation of human neural precursor cells. We acknowledge use of the Central Imaging and Flow Cytometry Facility (CIFF), Stem Cell Culture Facility and Biosafety level-2 laboratory facility at NCBS, TIFR.

AUTHOR CONTRIBUTIONS

P.C. and B.K.D performed the experiments and analysed the data. P.C., G.H. and C.W.T. conceptualized the experiments and wrote the manuscript.

DECLARATION OF INTERESTS

The authors declare no competing interests.

REFERENCES

Agholme, L., Lindström, T., Kågedal, K., Marcusson, J. and Hallbeck, M. 2010. An in vitro model for neuroscience: differentiation of SH-SY5Y cells into cells with morphological and biochemical characteristics of mature neurons. *J. Alzheimer's Dis.* 20:1069–1082.

Agrawal, N., Venkiteswaran, G., Sadaf, S., Padmanabhan, N., Banerjee, S. and Hasan, G. 2010. Inositol 1, 4, 5-trisphosphate receptor and dSTIM function in *Drosophila* insulin-producing neurons regulates systemic intracellular calcium homeostasis and flight. *J. Neurosci*. 30:1301-1313.

Ahmad, M. et al. 2022. Functional communication between IP_3R and STIM2 at

subthreshold stimuli is a critical checkpoint for initiation of SOCE. *Proc. Natl. Acad. Sci.* 119: e2114928118.

Atakpa, P., Thillaiappan, N.B., Mataragka, S., Prole, D.L. and Taylor, C.W. 2018. IP_3 receptors preferentially associate with ER-lysosome contact sites and selectively deliver Ca^{2+} to lysosomes. *Cell Rep.* 25:3180-3193.

Auyeung, V.C., Ulitsky, I., McGeary, S.E. and Bartel, D.P. 2013. Beyond secondary structure: primary-sequence determinants license pri-miRNA hairpins for processing. *Cell.* 152:844-858.

Bartok, A., Weaver, D., Golenár, T., Nichtova, Z., Katona, M., Bánsághi, S., Alzayady, K.J., Thomas, V.K., Ando, H., Mikoshiba, K. and Joseph, S.K. 2019. IP_3 receptor isoforms differently regulate ER-mitochondrial contacts and local calcium transfer. *Nat. Commun*. 10:1-14.

Béliveau, É., Lessard, V. and Guillemette, G. 2014. STIM1 positively regulates the Ca^{2+} release activity of the inositol 1,4,5-trisphosphate receptor in bovine aortic endothelial cells. *PLoS One.* 9: e114718.

Broad, L.M., Braun, F.J., Lievremont, J.P., Bird, G.S.J., Kurosaki, T. and Putney Jr, J.W. 2001. Role of the phospholipase C-inositol 1, 4, 5-trisphosphate pathway in calcium release-activated calcium current and capacitative calcium entry. *J. Biol. Chem.* 276:15945–15952.

Carrasco, S. and Meyer, T. 2011. STIM proteins and the endoplasmic reticulum-plasma membrane junctions. *Annu. Rev. Biochem.* 80:973–1000.

Chakraborty, S., Deb, B.K., Chorna, T., Konieczny, V., Taylor, C.W. and Hasan, G. 2016. Mutant IP_3 receptors attenuate store-operated Ca^{2+} entry by destabilizing

356 STIM–Orai interactions in *Drosophila* neurons. *J. Cell Sci.* 129:3903–3910.

357 Chang, C.L., Hsieh, T.S., Yang, T.T., Rothberg, K.G., Azizoglu, D.B., Volk, E., Liao,
358 J.C. and Liou, J. 2013. Feedback regulation of receptor-induced Ca^{2+} signaling
359 mediated by E-Syt1 and Nir2 at endoplasmic reticulum-plasma membrane
360 junctions. *Cell Rep*. 5:813–825.

361 Darbellay, B., Arnaudeau, S., Bader, C.R., Konig, S. and Bernheim, L. 2011. STIM1L
362 is a new actin-binding splice variant involved in fast repetitive Ca^{2+} release. *J.*
363 *Cell Biol.* 194:335-346.

364 Deb, B. K., Pathak, T. and Hasan, G. 2016. Store-independent modulation of Ca^{2+}
365 entry through Orai by Septin 7. *Nat. Commun.* 7:1-15.

366 Dellis, O., Rossi, A.M., Dedos, S.G. and Taylor, C.W. 2008. Counting functional
367 inositol 1, 4, 5-trisphosphate receptors into the plasma membrane. *J Biol. Chem.*
368 283:751-755.

369 Derangère, V., Bruchard, M., Végran, F. and Ghiringhelli, F. 2016. Proximity Ligation
370 Assay (PLA) protocol using Duolink® for T cells. *Bio-protocol.* 6:e1811.

371 Forostyak, O., Romanyuk, N., Verkhratsky, A., Sykova, E. and Dayanithi, G. 2013.
372 Plasticity of calcium signaling cascades in human embryonic stem cell-derived
373 neural precursors. *Stem Cells Dev.* 22:1506-1521.

374 Foskett, J.K., White, C., Cheung, K.H. and Mak, D.O.D. 2007. Inositol trisphosphate
375 receptor Ca^{2+} release channels. *Physiol. Rev.* 87:593–658.

376 Giordano, F., Saheki, Y., Idevall-Hagren, O., Colombo, S.F., Pirruccello, M., Milosevic,
377 I., Gracheva, E.O., Bagriantsev, S.N., Borgese, N. and De Camilli, P. 2013. PI(4,
378 5) P_2-dependent and Ca^{2+}-regulated ER-PM interactions mediated by the

379 extended synaptotagmins. *Cell*. 153:1494-1509.

380 Gopurappilly, R., Deb, B.K., Chakraborty, P. and Hasan, G. 2018. Stable STIM1
381 knockdown in self-renewing human neural precursors promotes premature
382 neural differentiation. *Front. Mol. Neurosci.* 11:178.

383 Gopurappilly, R., Deb, B.K., Chakraborty, P. and Hasan, G. 2019. Measurement of
384 store-operated calcium entry in human neural cells: From precursors to
385 differentiated neurons. *Methods Mol. Biol.* 2029:257–271.

386 Grudt, T. J., Usowicz, M. M. and Henderson, G. 1996. Ca^{2+} entry following store
387 depletion in SH-SY5Y neuroblastoma cells. *Mol. Brain Res.* 36:93–100.

388 Grynkiewicz, G., Poenie, M. and Tsien, R. Y. 1985. A new generation of Ca^{2+}
389 indicators with greatly improved fluorescence properties. *J. Biol. Chem.*
390 260:3440–3450.

391 Iwai, M., Michikawa, T., Bosanac, I., Ikura, M. and Mikoshiba, K. 2007. Molecular
392 basis of the isoform-specific ligand-binding affinity of inositol 1, 4, 5-
393 trisphosphate receptors. *J. Biol. Chem.* 282:12755–12764.

394 Kang, F., Zhou, M., Huang, X., Fan, J., Wei, L., Boulanger, J., Liu, Z., Salamero, J.,
395 Liu, Y. and Chen, L. 2019. E-syt1 Re-arranges STIM1 clusters to stabilize ring-
396 shaped ER-PM contact sites and accelerate Ca^{2+} store replenishment. *Sci Rep.*
397 9:1-11.

398 Knapp, M.L., Förderer, K., Alansary, D., Jung, M., Schwarz, Y., Lis, A. and Niemeyer,
399 B.A. 2020. Alternative splicing switches STIM1 targeting to specialized
400 membrane contact sites and modifies SOCE. *bioRxiv*. doi:
401 10.1101/2020.03.25.005199. (Preprint posted January 1, 2020).

Knott, S.R., Maceli, A.R., Erard, N., Chang, K., Marran, K., Zhou, X., Gordon, A., El Demerdash, O., Wagenblast, E., Kim, S. and Fellmann, C. 2014. A computational algorithm to predict shRNA potency. *Mol. Cell.* 56:796-807.

Lewis, R. S. 2020. Store-operated calcium channels: From function to structure and back again. *Cold Spring Harb. Perspect. Biol.* 12: a035055.

Ma, H. T., Venkatachalam, K., Li, H. S., Montell, C., Kurosaki, T., Patterson, R. L., & Gill, D. L. 2001. Assessment of the role of the inositol 1,4,5-trisphosphate receptor in the activation of transient receptor potential channels and store-operated Ca^{2+} entry channels. *J Biol Chem*, 276: 18888–18896.

Ma, H. T., Venkatachalam, K., Parys, J. B., & Gill, D. L. 2002. Modification of store-operated channel coupling and inositol trisphosphate receptor function by 2-aminoethoxydiphenyl borate in DT40 lymphocytes. *J Biol Chem*, 277: 6915–6922.

Maléth, J., Choi, S., Muallem, S. and Ahuja, M. 2014. Translocation between PI(4, 5)P_2-poor and PI(4, 5)P_2-rich microdomains during store depletion determines STIM1 conformation and Orai1 gating. *Nat Commun.* 5:1–10.

Mataragka, S. and Taylor, C. W. 2018. All three IP_3 receptor subtypes generate Ca^{2+} puffs, the universal building blocks of IP_3-evoked Ca^{2+} signals. *J Cell Sci.* 131: jcs220848.

Miotke, L., Lau, B. T., Rumma, R. T., & Ji, H. P. 2014. High sensitivity detection and quantitation of DNA copy number and single nucleotide variants with single color droplet digital PCR. *Anal. Chem.*, *86:* 2618-2624.

Nunes-Hasler, P., Maschalidi, S., Lippens, C., Castelbou, C., Bouvet, S., Guido, D.,

425 Bermont, F., Bassoy, E.Y., Page, N., Merkler, D. and Hugues, S. 2017. STIM1
426 promotes migration, phagosomal maturation and antigen cross-presentation in
427 dendritic cells. *Nat Commun*. 8:1-15.
428 Okeke, E., Parker, T., Dingsdale, H., Concannon, M., Awais, M., Voronina, S., Molgó,
429 J., Begg, M., Metcalf, D., Knight, A.E. and Sutton, R. 2016. Epithelial–
430 mesenchymal transition, IP_3 receptors and ER–PM junctions: Translocation of
431 Ca^{2+} signalling complexes and regulation of migration. *Biochem. J*. 473:757–767.
432 Palty, R., Raveh, A., Kaminsky, I., Meller, R. and Reuveny, E. 2012. SARAF
433 inactivates the store operated calcium entry machinery to prevent excess
434 calcium refilling. *Cell*. 149:425-438.
435 Parekh, A. B. and Putney, J. W. 2005. Store-operated calcium channels. *Physiol. Rev.*
436 85:757–810.
437 Parekh, A. B., Riley, A. M. and Potter, B. V. L. 2002. Adenophostin A and ribophostin,
438 but not inositol 1,4,5-trisphosphate or manno-adenophostin, activate the Ca^{2+}
439 release-activated Ca^{2+} current, ICRAC, in weak intracellular Ca^{2+} buffer.
440 *Biochem. J*. 361:133–141.
441 Patt, J., Alenfelder, J., Pfeil, E.M., Voss, J.H., Merten, N., Eryilmaz, F., Heycke, N.,
442 Rick, U., Inoue, A., Kehraus, S. and Deupi, X. 2021. An experimental strategy to
443 probe Gq contribution to signal transduction in living cells. *J. Biol. Chem.*
444 296:100472.
445 Poteser, M., Leitinger, G., Pritz, E., Platzer, D., Frischauf, I., Romanin, C. and
446 Groschner, K. 2016. Live-cell imaging of ER-PM contact architecture by a novel
447 TIRFM approach reveals extension of junctions in response to store-operated

Ca^{2+}-entry. *Sci. Rep*. 6:1-13.

Prakriya, M. and Lewis, R. S. 2001. Potentiation and inhibition of Ca^{2+} release-activated Ca^{2+} channels by 2-aminoethyldiphenyl borate (2-APB) occurs independently of IP_3 receptors. *J Physiol*. 536:3–19.

Prakriya, M. and Lewis, R. S. 2015. Store-operated calcium channels pharmacology. *Physiol. Rev.* 307:1383–1436.

Prole, D. L. and Taylor, C. W. 2019. Structure and function of IP_3 receptors. *Cold Spring Harb. Perspect. Biol.* 11: a035063.

Putney, J. W. 1986. A model for receptor-regulated calcium entry. *Cell Calcium*. 7:1–12.

Ran, F. A., Hsu, P. D., Wright, J., Agarwala, V., Scott, D. A., & Zhang, F. 2013. Genome engineering using the CRISPR-Cas9 system. *Nat. Protoc*. 8: 2281-2308.

Rana, A., Yen, M., Sadaghiani, A.M., Malmersjö, S., Park, C.Y., Dolmetsch, R.E. and Lewis, R.S. 2015. Alternative splicing converts STIM2 from an activator to an inhibitor of store-operated calcium channels. *J Cell Biol.* 209: 653-670.

Reinhardt, P., Glatza, M., Hemmer, K., Tsytsyura, Y., Thiel, C.S., Höing, S., Moritz, S., Parga, J.A., Wagner, L., Bruder, J.M. and Wu, G. 2013. Derivation and expansion using only small molecules of human neural progenitors for neurodegenerative disease modeling. *PLoS One.* 8: e59252.

Rosado, J.A., Diez, R., Smani, T. and Jardín, I. 2016. STIM and Orai1 variants in store-operated calcium entry. *Front. Pharmacol.* 6:325.

Rosado, J. A., Jenner, S. and Sage, S. O. 2000. A role for the actin cytoskeleton in

the initiation and maintenance of store-mediated calcium entry in human platelets. Evidence for conformational coupling. *J Biol. Chem*. 275: 7527–7533.

Saleem, H., Tovey, S.C., Rahman, T., Riley, A.M., Potter, B.V. and Taylor, C.W. 2013. Stimulation of inositol 1, 4, 5-trisphosphate (IP_3) receptor subtypes by analogues of IP_3. *PLoS One.* 8:e54877.

Sampieri, A., Santoyo, K., Asanov, A. and Vaca, L. 2018. Association of the IP_3R to STIM1 provides a reduced intraluminal calcium microenvironment, resulting in enhanced store-operated calcium entry. *Sci Rep*. 8:1–13.

Santoso, N. G., Cebotaru, L. and Guggino, W. B. 2011. Polycystin-1, 2, and STIM1 interact with IP_3R to modulate ER Ca^{2+} release through the PI3K/Akt pathway. *Cell Physiol Biochem*. 27:715–726.

Srivats, S., Balasuriya, D., Pasche, M., Vistal, G., Edwardson, J.M., Taylor, C.W. and Murrell-Lagnado, R.D. 2016. Sigma-1 receptors inhibit store-operated Ca^{2+} entry by attenuating coupling of STIM1 to Orai1. *J. Cell Biol.* 213: 65–79.

Sugawara, H., Kurosaki, M., Takata, M. and Kurosaki, T. 1997. Genetic evidence for involvement of type 1, type 2 and type 3 inositol 1, 4, 5-trisphosphate receptors in signal transduction through the B-cell antigen receptor. *EMBO J*. 16:3078–3088.

Thillaiappan, N.B., Chavda, A.P., Tovey, S.C., Prole, D.L. and Taylor, C.W. 2017. Ca^{2+} signals initiate at immobile IP_3 receptors adjacent to ER-plasma membrane junctions. *Nat. Commun.* 8:1-16.

Thillaiappan, N.B., Chakraborty, P., Hasan, G. and Taylor, C.W. 2019. IP_3 receptors and Ca^{2+} entry. *Biochim Biophys Acta Mol Cell Res*. 1866:1092–1100.

494 Tovey, S.C., De Smet, P., Lipp, P., Thomas, D., Young, K.W., Missiaen, L., De Smedt,
495 H., Parys, J.B., Berridge, M.J., Thuring, J. and Holmes, A. 2001. Calcium puffs
496 are generic $InsP_3$-activated elementary calcium signals and are downregulated
497 by prolonged hormonal stimulation to inhibit cellular calcium responses. *J. Cell*
498 *Sci*. 114:3979-3989.
499 Venkiteswaran, G. and Hasan, G. 2009. Intracellular Ca^{2+} signaling and store-
500 operated Ca^{2+} entry are required in *Drosophila* neurons for flight. *Proc. Natl.*
501 *Acad. Sci. U. S. A.* 106:10326–10331.
502 Wojcikiewicz, R. J. H. 1995. Type I, II, and III inositol 1,4,5-trisphosphate receptors
503 are unequally susceptible to down-regulation and are expressed in markedly
504 different proportions in different cell types. *J. Biol. Chem*. 270:11678–11683.
505 Woo, J.S., Sun, Z., Srikanth, S. and Gwack, Y. 2020. The short isoform of extended
506 synaptotagmin-2 controls Ca^{2+} dynamics in T cells via interaction with STIM1.
507 *Sci. Rep*. 10:1-13.
508 Woodard, G.E., López, J.J., Jardín, I., Salido, G.M. and Rosado, J.A. 2010. TRPC3
509 regulates agonist-stimulated Ca^{2+} mobilization by mediating the interaction
510 between type I inositol 1, 4, 5-trisphosphate receptor, RACK1, and Orai1. *J. Biol.*
511 *Chem*. 285: 8045–8053.
512 Yoshikawa, F., Morita, M., Monkawa, T., Michikawa, T., Furuichi, T. and Mikoshiba, K.
513 1996. Mutational analysis of the ligand binding site of the inositol 1, 4, 5-
514 trisphosphate receptor. *J. Biol. Chem.* 271:18277-18284.
515 Yue, L., Wang, L., Du, Y., Zhang, W., Hamada, K., Matsumoto, Y., Jin, X., Zhou, Y.,
516 Mikoshiba, K., Gill, D.L. and Han, S. 2020. Type 3 inositol 1, 4, 5-trisphosphate

receptor is a crucial regulator of calcium dynamics mediated by endoplasmic reticulum in HEK cells. *Cells*. 9:275.

519 **Figure 1. Loss of IP_3R1 Attenuates SOCE in Human Neural Stem Cells**

520 (A) Confocal images of hNPCs (passage 6) stained for DAPI and neural stem cell

521 proteins: Pax6 and Ki67 (proliferation marker). Scale bars, 50 μm.

522 (B) WB for IP_3R1 of hNPCs expressing non-silencing (NS) or IP_3R1-shRNA.

523 (C) Summary results (mean ± s.d., $n = 3$) show IP_3R1 expression relative to actin. $^{**}P$

524 < 0.01, Student's *t*-test with unequal variances.

525 (D) Changes in $[Ca^{2+}]_c$ evoked by thapsigargin (Tg, 10 μM) in Ca^{2+}-free HBSS and

526 then restoration of extracellular Ca^{2+} (2 mM) in hNPCs expressing NS or IP_3R1-

527 shRNA. Mean ± s.e.m. from 3 independent experiments, each with 4 replicates that

528 together included 100-200 cells. Inset shows the target of Tg.

529 (E-G) Summary results (individual cells, median (bar), 25^{th} and 75^{th} percentiles (box)

530 and mean (circle)) show Ca^{2+} signals evoked by Tg or Ca^{2+} restoration (E), rate of

531 Ca^{2+} entry (F) and resting $[Ca^{2+}]_c$ (G). $^{***}P < 0.001$, Mann-Whitney U-test.

532 (H) Changes in $[Ca^{2+}]_c$ evoked by Tg (10 μM) in Ca^{2+}-free HBSS and after restoring

533 extracellular Ca^{2+} (2 mM) in neurons (differentiated hNPCs) expressing NS or IP_3R1-

534 shRNA. Mean ± s.e.m. from 3 experiments with 100-200 cells.

535 (I,J) Summary results (presented as in E-G) show Ca^{2+} signals evoked by Tg or Ca^{2+}

536 restoration (I) and rate of Ca^{2+} entry (J). $^{***}P < 0.001$. Mann-Whitney U-test.

537 See also **Figure S1.**

538

Figure 2. Loss of IP_3R1 Attenuates SOCE in SH-SY5Y Cells

(A) WB for IP_3R1-3 of SH-SY5Y cells expressing non-silencing (NS) or IP_3R1-shRNA.

(B) Summary results (mean ± s.d., $n = 4$) show IP_3R expression relative to actin normalized to control NS cells. $^{**}P < 0.01$, Student's *t*-test with unequal variances.

(C) Ca^{2+} signals evoked by carbachol (CCh, 3 μM) in SH-SY5Y cells expressing NS or IP_3R1-shRNA. Mean ± s.e.m. from 3 experiments with 100-200 cells.

(D) Summary results show peak changes in $[Ca^{2+}]_c$ ($\Delta[Ca^{2+}]_c$) evoked by CCh. $^{***}P < 0.001$, Mann-Whitney U-test.

(E) Ca^{2+} signals evoked by thapsigargin (Tg, 10 μM) in Ca^{2+}-free HBSS and then after restoration of extracellular Ca^{2+} (2 mM) in cells expressing NS or IP_3R1-shRNA. Mean ± s.e.m. from 3 experiments with 50-100 cells.

(F, G) Summary results (individual cells, mean ± s.e.m., $n = 3$, 50-100 cells) show peak changes in $[Ca^{2+}]_c$ evoked by Ca^{2+} restoration ($\Delta[Ca^{2+}]_c$) (F) and rate of Ca^{2+} entry (G). $^{***}P < 0.001$, Mann-Whitney U-test.

(H) Ca^{2+} signals evoked by Tg and then Ca^{2+} restoration in cells expressing NS-shRNA, or IP_3R1-shRNA alone or with IP_3R1 or IP_3R3. Traces show mean ± s.e.m. (100-220 cells from 3 experiments).

(I, J) Summary results (mean ± s.e.m, 100-220 cells from 3 experiments) show peak increases in $[Ca^{2+}]_c$ ($\Delta[Ca^{2+}]_c$) evoked by Ca^{2+} restoration (I) and rates of Ca^{2+} entry (J) evoked by restoring extracellular Ca^{2+}.

(K) Effects of thapsigargin (Tg, 10 μM) in Ca^{2+}-free HBSS and then after Ca^{2+} restoration (2 mM) in cells expressing IP_3R1-shRNA alone or with IP_3R1 or mCh-STIM1. Traces show mean ± s.e.m. (100-150 cells from 3 experiments).

562 (L, M) Summary results (mean ± s.e.m.) show peak increase in $[Ca^{2+}]_c$ after Ca^{2+}

563 restoration ($\Delta[Ca^{2+}]_c$) (L) and rate of Ca^{2+} entry (M). Different letters indicate significant

564 differences (panels I, J, L, M), $P < 0.001$, one-way ANOVA with pair-wise Tukey's test.

565 See also **Figures S2-S4.**

566

567

568

Figure 3. Regulation of SOCE by IP_3R Requires IP_3 Binding But Not a Functional Pore in SH-SY5Y cells

(A) SOCE is activated when loss of Ca^{2+} from the ER through IP_3Rs activates STIM1 (i). Our results suggest an additional role for IP_3Rs (ii).

(B) SH-SY5Y cells expressing IP_3R1-shRNA alone or with IP_3R1 or IP_3R1^{DA} were stimulated with thapsigargin (Tg, 1 µM) in Ca^{2+}-free HBSS before restoring extracellular Ca^{2+} (2 mM). Traces show mean ± s.e.m, for 100-150 cells from 3 experiments.

(C) Cells expressing IP_3R1-shRNA and IP_3R1^{DA} were treated with NS-siRNA or Orai1-siRNA before measuring Tg-evoked Ca^{2+} entry. Traces show mean ± s.e.m. for 85-100 cells from 3 experiments.

(D) Summary results (mean ± s.e.m.) show peak increases in $[Ca^{2+}]_c$ ($\Delta[Ca^{2+}]_c$) evoked by Ca^{2+} restoration.

(E) Tg-evoked Ca^{2+} entry in cells expressing IP_3R1-shRNA with IP_3R1, IP_3R1^{RQ} or $IP_3R1^{RQ/KQ}$. Traces show mean ± s.e.m, for 90-150 cells from 3 experiments.

(F) Summary results (mean ± s.e.m.) show peak increases in $[Ca^{2+}]_c$ ($\Delta[Ca^{2+}]_c$) evoked by Ca^{2+} restoration. Different letter codes (panels D, F) indicate significantly different values, $P < 0.001$, one-way ANOVA and pair-wise Tukey's test.

See also **Figure S5.**

Figure 4. Receptor-Regulated IP_3 Production Stimulates SOCE in Cells With Empty Ca^{2+} Stores and Expressing Pore-Dead IP_3R

(A, B) SH-SY5Y cells expressing IP_3R1-shRNA alone (A) or with IP_3R1^{DA} (B) were treated with a low concentration of CPA (2 µM) in Ca^{2+}-free HBSS to partially deplete the ER of Ca^{2+} and sub-maximally activate SOCE (see **Figures S5M and S5N**). Carbachol (CCh, 1 µM) was then added to stimulate IP_3 formation through muscarinic receptors, and extracellular Ca^{2+} (2 mM) was then restored. Traces (mean ± s.e.m of 113-200 cells from 3 experiments) show responses with and without the CCh addition.

(C) Summary results show the peak increases in $[Ca^{2+}]_c$ ($\Delta[Ca^{2+}]_c$) after addition of CCh (CCh-induced Ca^{2+} release) and then after restoring extracellular Ca^{2+} (SOCE).

(D-F) SH-SY5Y cells wild type (WT) (D) and expressing NS-shRNA (E) or IP_3R1-shRNA (F) were treated with YM-254890 (YM, 1 µM, 5 min) in Ca^{2+}-free HBSS to inhibit Gαq and then with thapsigargin (Tg, 1 µM) before restoring extracellular Ca^{2+} (2 mM). Traces show mean ± s.e.m of 80 -100 cells from 3 experiments. .

(G-I) Similar analyses of HEK 293T cells. Summary results (mean ± s.e.m, 50-100 cells from 3 experiments) are shown in (I).

Different letter codes (panels C and I) indicate significantly different values within the store Ca^{2+} release or SOCE groups, $P < 0.001$, one-way ANOVA and pair-wise Tukey's test.

See also **Figure S6.**

Figure 5. IP_3Rs Promote Interaction of STIM1 With Orai1

(A-E) PLA analyses of interactions between STIM1 and Orai1 in SH-SY5Y cells expressing NS-shRNA (A) or IP_3R1-shRNA alone (B) or with IP_3R1 (C), IP_3R1^{DA} (D) or $IP_3R1^{RQ/KQ}$ (E). Confocal images are shown for control cells or after treatment with thapsigargin (Tg, 1 µM) in Ca^{2+}-free HBSS. PLA reaction product is red, and nuclei are stained with DAPI (blue). Scale bars, 5 µm. Summary results show the surface area of the PLA spots for 8-10 cells from 2 independent analyses. Individual values, median (bar) and 25th and 75th percentiles (box). $^{***}P < 0.001$, Student's *t*-test with unequal variances.

See also **Figure S7.**

Figure 6. Extended Synaptotagmins Rescue SOCE in Cells Lacking IP_3R1

(A) SH-SY5Y cells expressing IP_3R1-shRNA alone or with E-Syt1 were stimulated with Tg (1 μM) in Ca^{2+}-free HBSS before restoring extracellular Ca^{2+} (2 mM). Traces show mean ± s.e.m, for 50-80 cells from 3 experiments.

(B) Summary results show $\Delta[Ca^{2+}]_c$ evoked by restoring Ca^{2+} (SOCE). Mean ± s.e.m, $^{***}P < 0.001$, Mann-Whitney U- test.

(C) Summary results (mean ± s.e.m, n = 50-80 cells) show resting $[Ca^{2+}]_c$ (left) and the peak Ca^{2+} signals ($\Delta[Ca^{2+}]_c$) evoked by thapsigargin (Tg, 1 μM) in Ca^{2+}-free HBSS for SH-SY5Y cells expressing IP_3R1-shRNA alone or with human E-Syt1.

(D) Cells over-expressing E-Syt1 and treated with IP_3R1-shRNA in combination with either NS or STIM1 siRNA were stimulated with Tg (1 μM) in Ca^{2+}-free HBSS before restoration of extracellular Ca^{2+} (2 mM). Mean ± s.e.m. from 3 experiments with 30-50 cells.

(E, F) Summary results (mean ± s.e.m, n = 30-50 cells) show SOCE evoked by Tg (E), resting $[Ca^{2+}]_c$ and the Tg-evoked Ca^{2+} release from intracellular stores (F). $^{***}P < 0.001$, one-way ANOVA with pair-wise Tukey's test.

(G) Similar analyses of cells expressing NS shRNA alone or with human E-Syt1 and then treated with Tg (1 μM) in Ca^{2+}-free HBSS before restoring extracellular Ca^{2+} (2 mM). Mean ± s.e.m. from 3 experiments with 75-110 cells.

(H, I) Summary results (mean ± s.e.m, n = 75-110) show resting $[Ca^{2+}]_c$ (H) and $\Delta[Ca^{2+}]_c$ evoked by Tg (store release) or Ca^{2+} restoration (SOCE) (I). No significant difference, one-way ANOVA with pair-wise Tukey's test.

Figure 7. Dual Regulation of SOCE by IP_3Rs

(A) SOCE is activated when loss of Ca^{2+} from the ER, usually mediated by opening of IP_3Rs when they bind IP_3, causes STIM to unfurl cytosolic domains (2). The exposed cytosolic domains of STIM1 reach across a narrow gap between the ER and PM at a MCS to interact with PIP_2 and Orai1 in the PM. Binding of STIM1 to Orai1 causes pore opening, and SOCE then occurs through the open Orai1 channel. We show that IP_3Rs when they bind IP_3 also facilitate interactions between Orai1 and STIM, perhaps by stabilizing the MCS (1). Receptors that stimulate IP_3 formation thereby promote both activation of STIM (by emptying Ca^{2+} stores) and independently promote interaction of active STIM1 with Orai1.

(B) Other mechanisms, including ryanodine receptors (RyR), can also release Ca^{2+} from the ER. We suggest that convergent regulation of SOCE by IP_3R with bound IP_3 allows receptors that stimulate IP_3 formation to selectively control SOCE.

STAR METHODS

RESOURCE AVAILABILITY

Lead Contact

All requests for resources and reagents should be directed to the lead contact, Dr. Gaiti Hasan (gaiti@ncbs.res.in).

Materials Availability

Constructs and cell lines are available upon request. MTA required for cell lines.

Data and Code Availability

This study did not generate any computer code. The data supporting the findings of this study are available within the manuscript. All other data supporting the findings of this study are available from the corresponding author on reasonable request.

METHOD DETAILS

Culture of Human Neural Precursor Cells

Human neural precursor cells (hNPCs) were derived from a human embryonic stem cell (hESC) line, H9/WA09, using a protocol that inhibits dual SMAD signaling and stimulates Wnt signaling (Reinhardt *et al.*, 2013) as described previously (Gopurappilly *et al.*, 2018, 2019). hNPCs were grown as adherent dispersed cells on growth factor-reduced Matrigel (0.5%) in hNPC maintenance medium (NMM) at 37°C in humidified air with 5% CO_2. NMM comprised a 1:1 mixture of DMEM/F-12 and

Neurobasal medium, supplemented with GlutaMAX (0.5x), N2 supplement (1:200), B27 without vitamin A (1:100), Antibiotic-Antimycotic, CHIR99021 (3 μM), purmorphamine (0.5 mM) and ascorbic acid (150 μM). Doubling time was ~24 hr. Cells were passaged every 4-5 days by treatment with StemPro accutase, stored in liquid nitrogen, and thawed as required. Cells were confirmed to be mycoplasma-free by monthly screening (MycoAlert). hNPCs between passages 16-19 were used. All experiments performed with hESC lines were approved by the Institutional Committee for Stem Cell Research, registered under the National Apex Committee for Stem Cell Research and Therapy, Indian Council of Medical Research, Ministry of Health, New Delhi.

Stable Knockdown of IP_3R1

An UltramiR lentiviral inducible shRNA-mir based on the shERWOOD algorithm (Auyeung *et al.*, 2013; Knott *et al.*, 2014) was used to inhibit IP_3R1 expression. The all-in-one pZIP vector, which allows puromycin-selection and doxycycline-induced expression of both shRNA-mir and Zs-Green for visualization, was from TransOMIC Technologies. Lentiviral pZIP transfer vectors encoding non-silencing shRNA (NS) or IP_3R1-targeting shRNA were packaged as lentiviral particles using packaging (pCMV-dR8.2 dpvr) and envelope vectors (pCMV-VSV-G) by transfection of HEK 293T cells. Viral particles were collected and processed, and hNPCs (passage 9) or SH-SY5Y cells were transduced (multiplicity of infection, MOI = 10) using Lipofectamine LTX with PLUS reagent. Cells were maintained in media containing doxycycline (2 μg/ml) to induce shRNA expression, and puromycin to select transduced cells (1 μg/ml for

hNPCs; 3 µg/ml for SH-SY5Y and HEK 293T cells). Cells were passaged 4-5 times after lentiviral transduction to select for stable expression of shRNAs.

Derivation of Neurons From hNPCs

Neurons were differentiated from hNPCs stably transduced with shRNA. hNPCs were seeded at 50-60% confluence in NMM on coverslips coated with poly-D-lysine (0.2 mg/ml). After 1-2 days, the medium was replaced with neuronal differentiation medium, which comprised a 1:1 mixture of DMEM/F-12 with Neurobasal supplemented with B27 (1:100), N2 (1:200), GlutaMAX (0.5x) and Antibiotic-Antimycotic solution. Medium was replaced on alternate days. Neurons were used after 15-20 days.

Culture and Transfection of SH-SY5Y Cells

SH-SY5Y cells were grown on culture dishes in DMEM/F-12 with 10% foetal bovine serum at 37 °C in humidified air with 5% CO_2. Cells were passaged every 3-4 days using TrypLE Express and confirmed to be free of mycoplasma. Cells expressing shRNA were transiently transfected using TransIT-LT1 transfection reagent in Opti-MEM. Plasmids (250 ng) and/or siRNA (200 ng) in transfection reagent (1 µg/2.5 µl) were added to cells grown to 50% confluence on glass coverslips attached to an imaging dish. Cells were used after 48 hr. The siRNAs used (100 nM) were to human Orai1 or non-silencing (NS), to human STIM1 or NS. The expression plasmids are described in Key Resources.

730 **CRISPR/Cas9n Editing of SH-SY5Y Cells**

731 To allow CRISPR/Cas9n-mediated disruption of IP_3R expression, we used a
732 published method to clone gRNAs into the backbone vector (pX459) (Ran *et al.*,
733 2013). Forward and reverse gRNA oligonucleotides (100 µM) were annealed and
734 ligated using T4 DNA ligase by incubation (10 µl, 37°C, 30 min) before slow cooling to
735 20°C. Plasmids encoding Cas9n were digested with *BbsI-HF* (37°C, 12 hr), gel-
736 purified (NucleoSpin Gel and PCR Clean-up kit) and the purified fragment was stored
737 at -20°C. A mixture (final volume 20 µl) of gRNA duplex (1 µl, 0.5 µM), digested pX459
738 vector (30 ng), 10× T4 DNA ligase buffer (2 µl) and T4 DNA ligase (1 µl) was
739 incubated (20°C, 1 hr). After transformation of DH5-α competent *E. coli* with the
740 ligation mixture, plasmids encoding Cas9n and the sgRNAs were extracted, and the
741 coding sequences were confirmed (Ran *et al.*, 2013). The plasmid (2 µg) was then
742 transfected into SH-SY5Y cells (50-60% confluent) in a 6-well plate using TransIT LT-
743 1 reagent. After 48 hr, puromycin (2.5 µg/ml, 72 hr) was added to kill non-transfected
744 cells. Colonies were then propagated and screened for the Ca^{2+} signals evoked by
745 carbachol and for the presence of the IP_3R gene by genomic DNA PCR and droplet
746 digital PCR using primers close to the region targeted by the gRNAs (as described in
747 Miotke *et al.*, 2014). Three independently derived lines, each with one residual IP_3R1
748 gene, were used for analyses of Ca^{2+} signaling (see **Figure S2I**). For one of the cell
749 lines (IKO 2), disruption of one copy of the IP_3R1 gene was confirmed by genomic
750 PCR, droplet digital PCR and Western blotting (**Figures S2F and S2G**).
751
752

Ca^{2+} Imaging

Methods for single-cell Ca^{2+} imaging were described previously (Gopurappilly *et al.*, 2019). Briefly, cells grown as a monolayer (~70% confluence) on homemade coverslip-bottomed dishes were washed and loaded with Fura 2 by incubation with Fura 2 AM (4 μM, 45 min, 37°C), washed and imaged at room temperature in HEPES-buffered saline solution (HBSS). HBSS comprised: 20 mM HEPES, 137 mM NaCl, 5 mM KCl, 2 mM $MgCl_2$, 2 mM $CaCl_2$, 10 mM glucose, pH 7.3. $CaCl_2$ was omitted from Ca^{2+}-free HBSS. Treatments with carbamoylcholine chloride (Carbachol, CCh), thapsigargin (Tg), cyclopiazonic acid (CPA), YM-254890 or high-K^+ HBSS (HBSS supplemented with 75 mM KCl) are described in legends.

Responses were recorded at 2-s intervals using an Olympus IX81-ZDC2 Focus Drift-Compensating Inverted Microscope with 60× oil immersion objective (numerical aperture, NA = 1.35) with excitation at 340 nm and 380 nm. Emitted light (505 nm) was collected with an Andor iXON 897E EMCCD camera and AndoriQ 2.4.2 imaging software. Maximal (R_{max}) and minimal (R_{min}) fluorescence ratios were determined by addition of ionomycin (10 μM) in HBSS containing 10 mM $CaCl_2$ or by addition of Ca^{2+}-free HBSS containing BAPTA (10 mM) and Triton X100 (0.1%). Background-corrected fluorescence recorded from regions of interest (ROI) drawn to include an entire cell was used to determine mean fluorescence ratios ($R = F_{340}/F_{380}$) (ImageJ), and calibrated to $[Ca^{2+}]_c$ from (Grynkiewicz, Poenie and Tsien, 1985):

$$[Ca^{2+}]_c = K_D \cdot \frac{F_{380}^{min}}{F_{380}^{max}} \cdot \frac{(R - R_{min})}{(R_{max} - R)}$$

where, K_D = 225 nM (Forostyak *et al.*, 2013).

775

776 **Western Blots**

777 Proteins were isolated in RIPA buffer with protease inhibitor cocktail or, for WB of
778 Orai1, in medium containing 150 mM NaCl, 50 mM Tris, 1% Triton-X-100, 0.1% SDS
779 and protease inhibitor cocktail. After 30 min on ice with intermittent shaking, samples
780 were collected by centrifugation (11,000 ×*g*, 20 min) and their protein content was
781 determined (BCA protein assay kit). Proteins (~30 µg/lane) were separated on 8%
782 SDS-PAGE gels for IP_3R or 10% SDS-PAGE gels for STIM1 and Orai1, and
783 transferred to a Protran 0.45-µm nitrocellulose membrane using a TransBlot semi-dry
784 transfer system. Membranes were blocked by incubation (1 hr, 20°C) in TBST
785 containing skimmed milk or BSA (5%). TBST (Tris-buffered saline with Tween)
786 comprised: 137 mM NaCl, 20 mM Tris, 0.1% Tween-20, pH 7.5. Membranes were
787 incubated with primary antibody in TBST (16 hr, 4°C), washed with TBST (3 ×10 min),
788 and incubated (1 hr, 20°C) in TBST containing HRP-conjugated secondary antibody.
789 After 3 washes, HRP was detected using ECL Western blotting substrate and
790 quantified using ImageQuant LAS 4000 and Image J. The primary antibodies used
791 and their dilutions are listed in Key Resources.

792

793 **Immunocytochemistry**

794 After appropriate treatments, cells on a coverslip-bottomed plate were washed twice
795 with cold PBS, fixed in PBS with paraformaldehyde (4%, 20°C, 20 min), washed (3 × 5
796 min) with PBS containing Triton-X100 (0.1%, PBST) and blocked by incubation (1 hr,
797 20°C) in PBST containing goat serum (5%). After incubation with primary antibody in

PBST (16 hr, 4°C) and washing with PBST (3 × 5 min), cells were incubated (1 hr, 20°C) with secondary antibody in PBST containing goat serum, washed (3 × 5 min), stained with DAPI (1 µg/ml in PBS, 10 min, 20°C) and washed (5 min, PBST). Cells were then covered with glycerol (60% v/v) and imaged using an Olympus FV300 confocal laser scanning microscope with 20× or 60× oil-immersion objectives. Fluorescence was analyzed using ImageJ. The primary antibodies used and their dilutions are provided in Key Resources.

Proximity Ligation Assay

The Duolink *In Situ* Red Starter Mouse/Rabbit kit was used according to the manufacturer's protocol with primary antibodies to Orai1 (mouse 1:500) and STIM1 (rabbit 1:1000). Cells (~30% confluent) were treated with thapsigargin (1 µM, 5 min) in Ca^{2+}-free HBSS before fixation, permeabilization, and incubation with primary antibodies (16 hr, 4°C) and the PLA reactants. Red fluorescent PLA signals were imaged using an Olympus FV300 confocal laser scanning microscope, with excitation at 561 nm, and a 60× oil-immersion objective. Quantitative analysis of the intensity and surface area of PLA spots used the "Analyze particle" plugin of Fiji. Results are shown for 8-10 cells from two biological replicates of each genotype.

Statistical Analyses

All experiments were performed without blinding or prior power analyses. Independent biological replicates are reported as the number of experiments (n), with the number of cells contributing to each experiment indicated in legends. The limited availability of

materials for PLA restricted the number of independent replicates (n) to 2 (each with 8-10 cells). Most plots show means ± s.e.m. (or s.d.). Box plots show 25th and 75th percentiles, median and mean (see legends). Where parametric analyses were justified by a Normality test, we used Student's *t*-test with unequal variances for 2-way comparisons and ANOVA followed by pair-wise Tukey's test for multiple comparisons. Non-parametric analyses used the Mann-Whitney U-test. Statistical significance is shown by $^{***}P < 0.001$, $^{**}P < 0.01$, $^{*}P < 0.05$, or by letter codes wherein different letters indicate significantly different values ($P < 0.001$, details in legends). All analyses used Origin 8.5 software.

Figure 1. Loss of IP_3R1 Attenuates SOCE in Human Neural Stem Cells

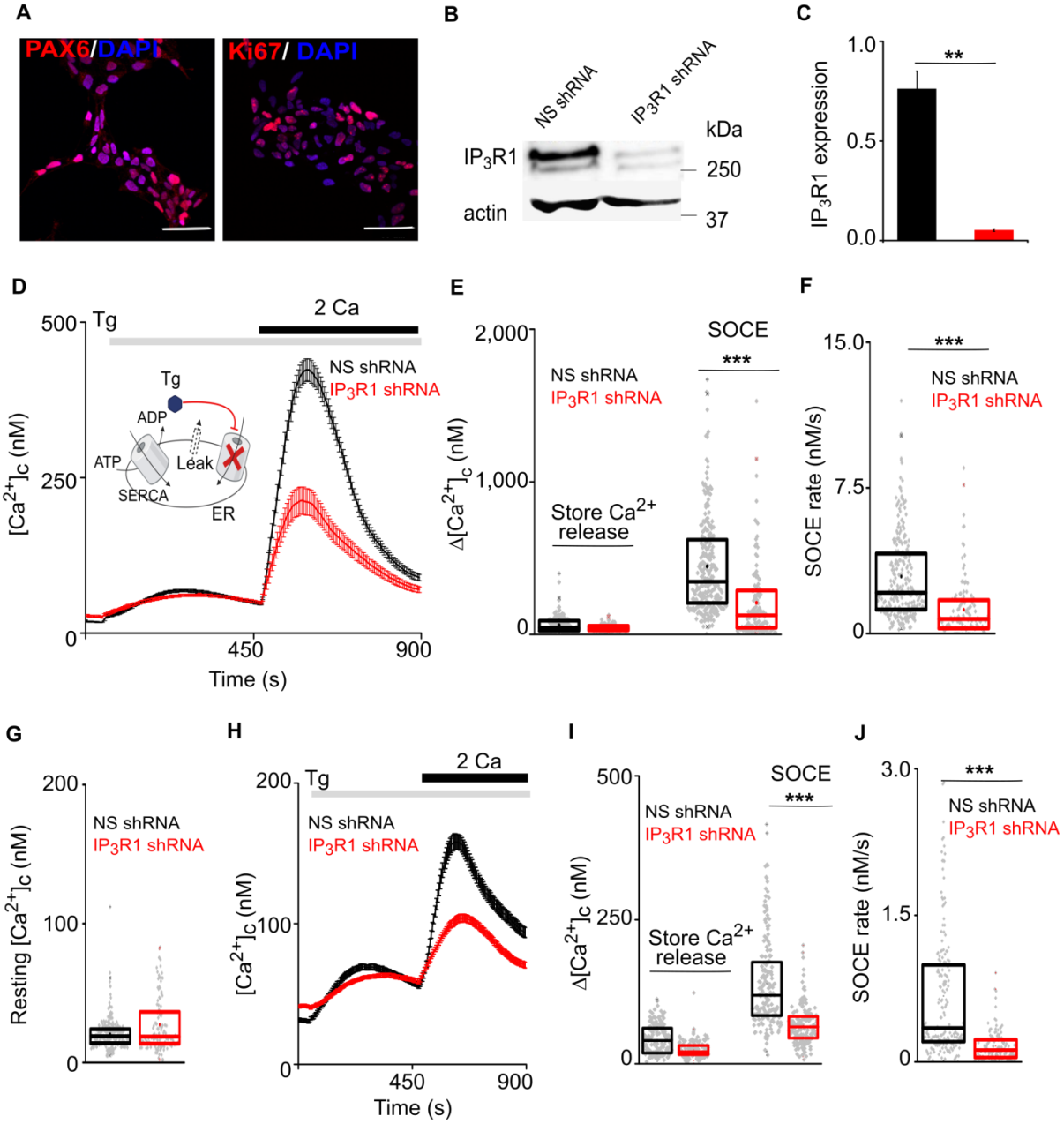

Figure 2. Loss of IP_3R1 Attenuates SOCE in SH-SY5Y Cells

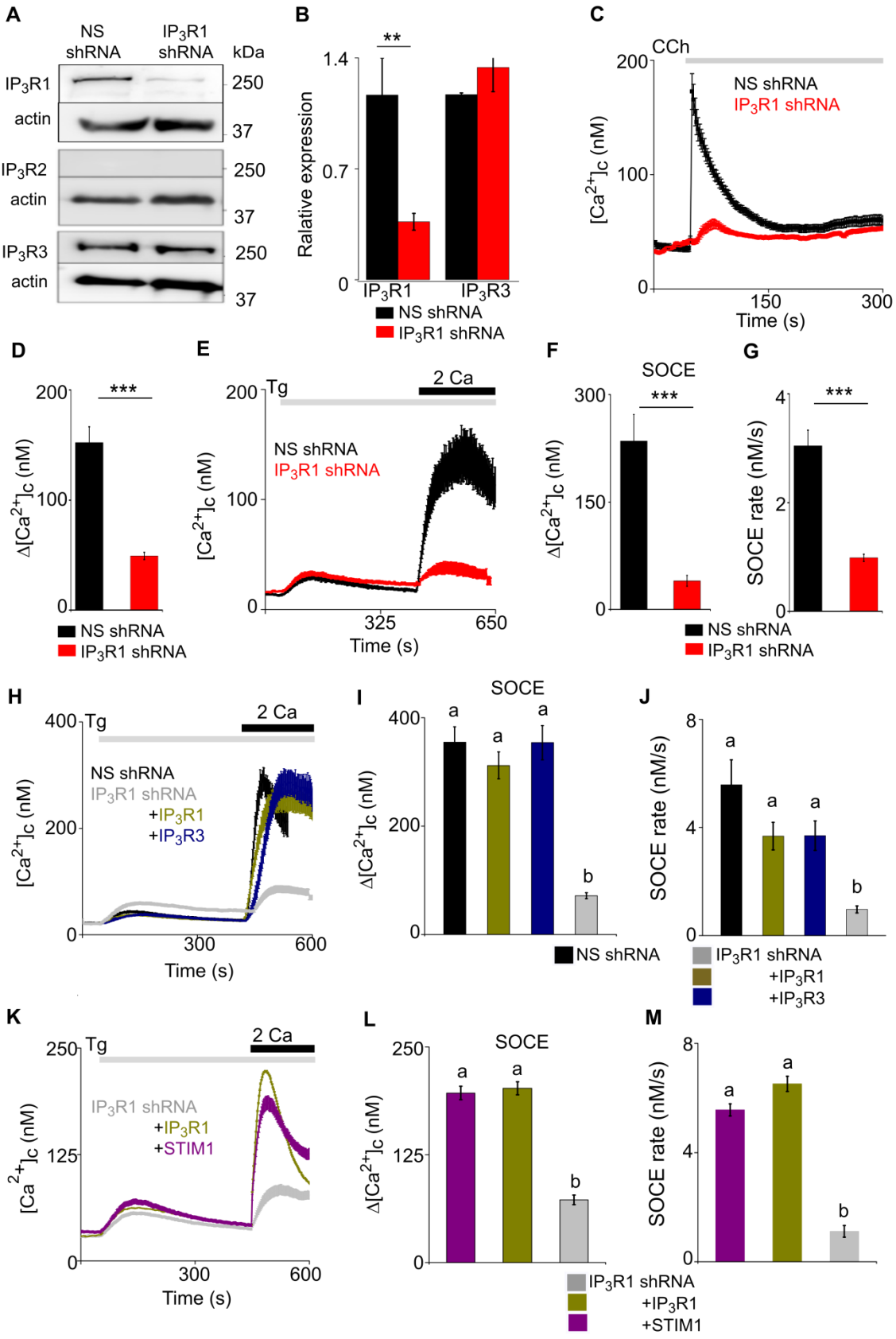

844

Figure 3. Regulation of SOCE by IP_3R Requires IP_3 Binding But Not a Functional Pore in SH-SY5Y cells

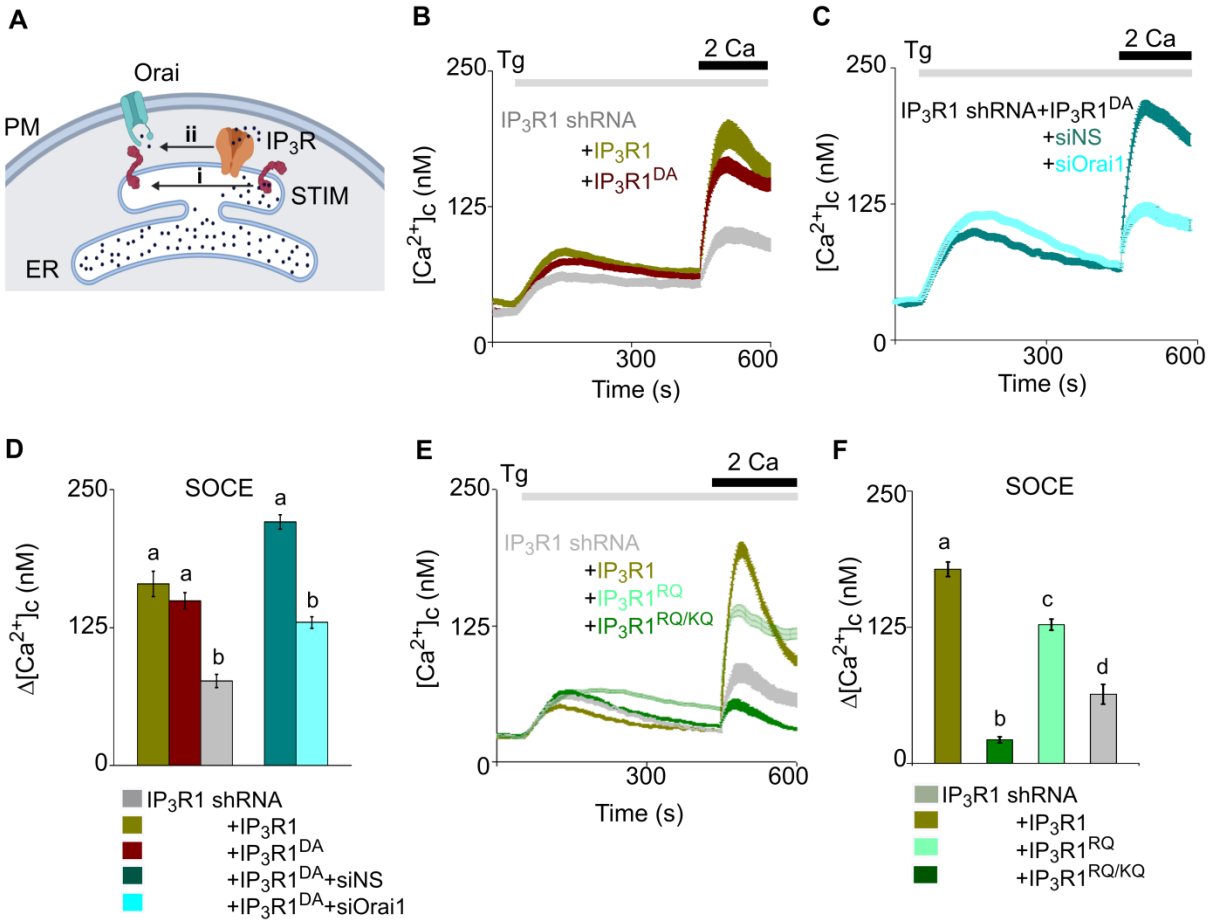

Figure 4. Receptor-Regulated IP_3 Production Stimulates SOCE in Cells with Empty Ca^{2+} Stores and Expressing Pore-Dead IP_3R

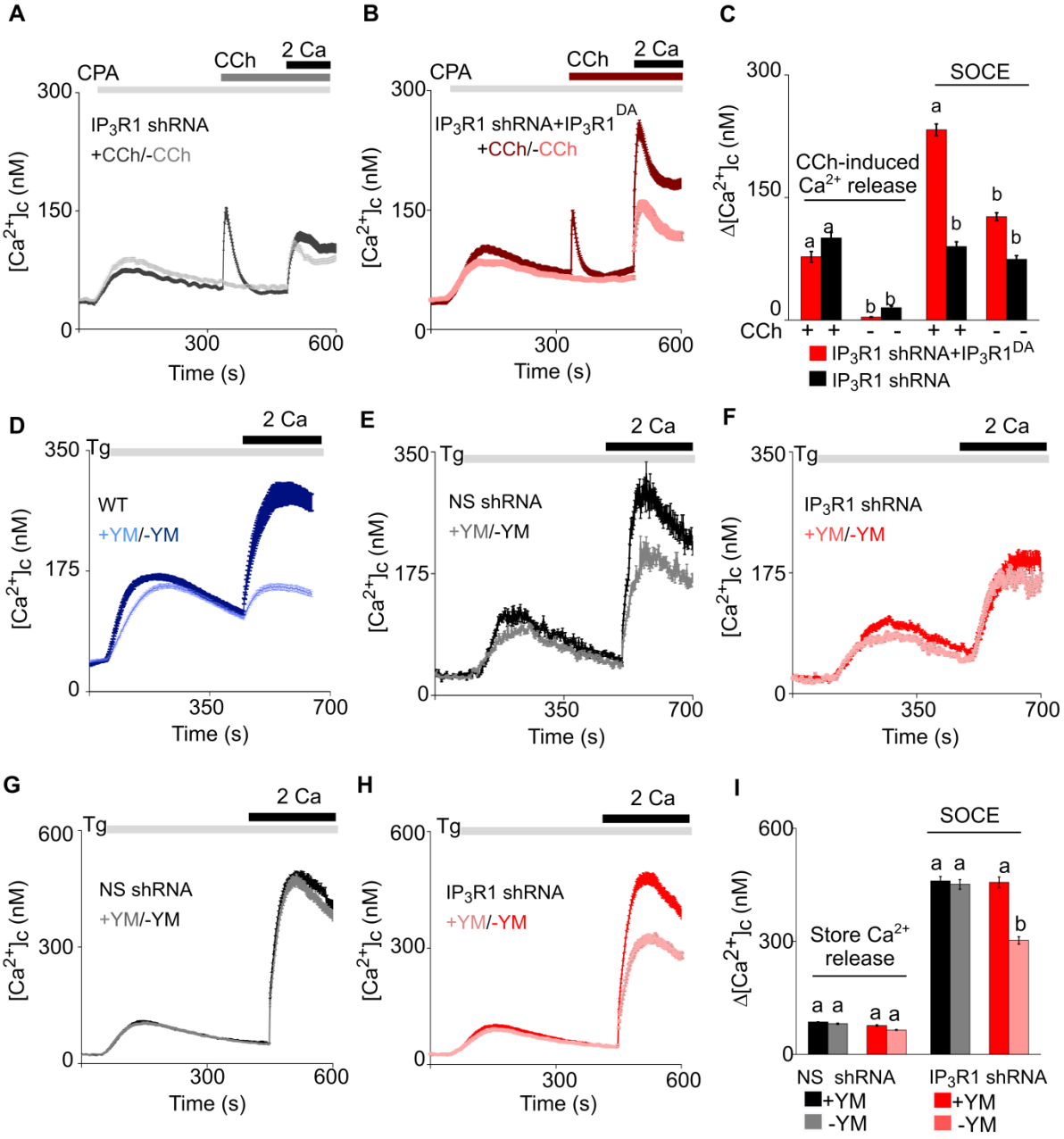

Figure 5. IP_3Rs Promote Interaction of STIM1 With Orai1

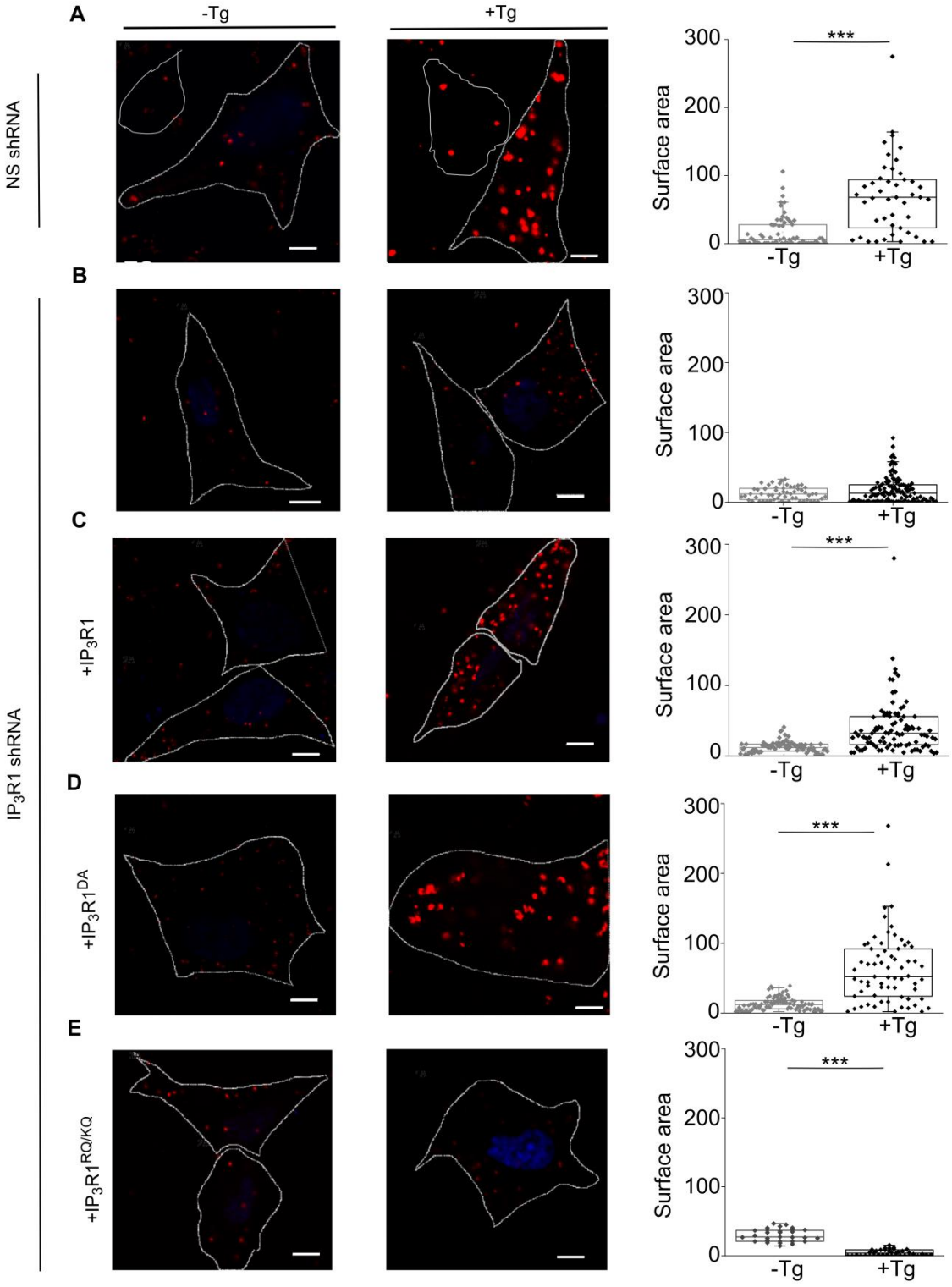

Figure 6. Extended Synaptotagmins Rescue SOCE in Cells Lacking IP_3R1

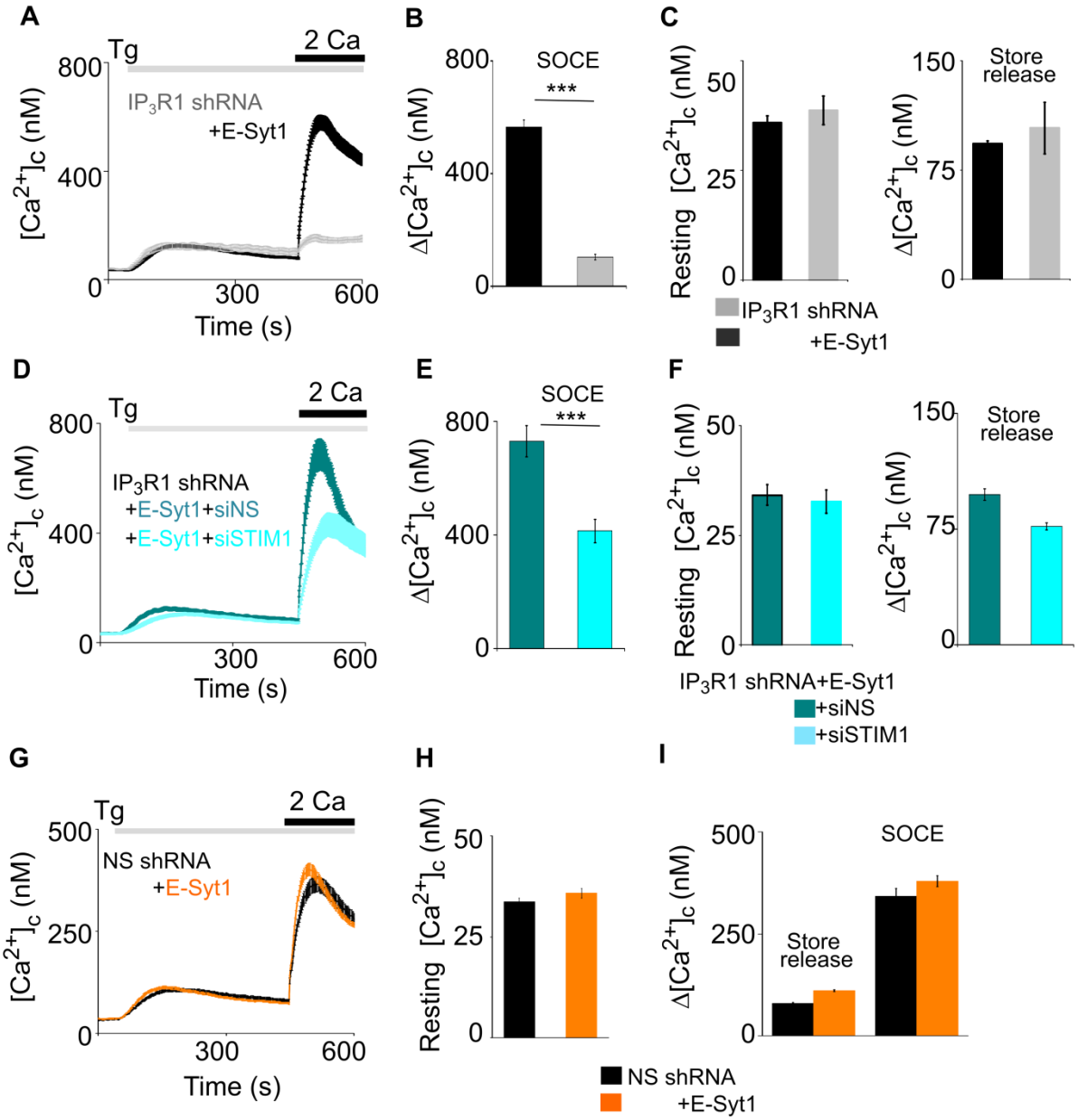

Figure 7. Dual Regulation of SOCE by IP_3Rs